Gap-junction coupling can prolong beta-cell burst period by an order of magnitude via phantom bursting

Alessandro Loppini[1] and Morten Gram Pedersen[2,3]

[1)] *Unit of Nonlinear Physics and Mathematical Modeling, Campus Bio-Medico University of Rome, I-00128 Rome, Italy.*

[2)] *Department of Information Engineering, University of Padua, I-35131 Padua, Italy.*

[3)] *Department of Mathematics "Tullio Levi-Civita", University of Padua, I-35131 Padua, Italy.*

(˙Dated: May 25, 2018)

Pancreatic β-cells show multiple intrinsic modes of oscillation with bursting electrical activity playing a crucial role. Bursting is seen both in experimentally isolated β-cells as well as in electrically coupled cells in the pancreatic islets, but the burst period is typically an order of magnitude greater in coupled cells. This difference has previously been attributed to noisier dynamics, or perturbed electrophysiological properties, in isolated β-cells. Here, we show that diffusive coupling alone can extend the period more than ten-fold in bursting oscillators modeled with a so-called phantom burster model, and analyze this result with slow-fast bifurcation analysis of an electrically coupled pair of cells. Our results should be applicable to other scenarios where coupling of bursting units, e.g. neurons, may increase the oscillation period drastically.

The endocrine pancreatic β-cells release insulin in distinct pulses as a result of bursting oscillatory activity in their membrane potentials, which arises from the interaction of slow and fast ion channel dynamics. Isolated β-cells typically show fast bursting oscillations, while electrically coupled β-cells within the pancreatic islets show a much slower bursting mode, which is believed to control the amount of insulin that is released. In this work, we show that different slow processes can work synergistically in coupled β-cells to regulate the bursting oscillation, leading to a $\sim$10-fold increase in the oscillation period. The result that gap-junction coupling alone can prolong the burst period to this extent represents a novelty with immediate implications for our understanding of emerging dynamics of β-cells underlying pulsatile insulin secretion. More generally, a coupling-controlled interplay of slow processes represents a new mechanism through which bursting oscillators may significantly increase their period to span several orders of magnitude, and may play a role also in other systems, such as neurons.

I. INTRODUCTION

Coupled oscillators are crucial components of dynamic systems in, e.g., physics, chemistry and biology, and the role of coupling has been widely studied to understand phenomena such as synchrony and oscillator death. The latter refers to oscillating units becoming stationary when coupled, a scenario observed in experiments and models of e.g. chemical oscillators[1,2] or biological cells[3,4]. Coupling can also promote biological oscillations by regularizing and synchronizing stochastic fluctuations occurring in single cells[5,6].

Bursting electrical activity is observed in many types of neurons and endocrine cells. It consists of action potential firing superimposed on a slower oscillation giving rise to groups of action potentials separated by silent phases. From a mathematical point of view, bursting results from the interplay between fast and slow variables, which can be analyzed by so-called slow-fast analysis[7]. Standard models of bursting have a single slow variable, which controls the switch between quiescence and activity[8–10].

The β-cells of the endocrine pancreas are a prototypical example of bursting cells, which have been studied extensively both experimentally and theoretically. Their periodic electrical activity is physiologically important since it drives pulsatile insulin release, which is

disturbed in diabetes[11–15]. Interesting, isolated β-cells typically exhibit continuous action potential firing (spiking) or very rapid bursting with a period of a few seconds, whereas electrically coupled β-cells located *in situ* in the pancreatic islets show bursting activity, and related Ca^{2+} oscillations, with a period of tens of seconds to minutes[16,17]. This difference in burst period has been attributed to various mechanisms. For example, noise has been suggested to shorten the bursts in isolated cells, but to be reduced in the electrically coupled β-cell population, allowing bursting to appear[18–23]. Alternatively, coupling alone can change spiking cells into bursters[24–27] and increase the burst period $\sim$2-fold in standard models of bursters[20,25,28]. Another possibility is that isolated β-cells have different electrophysiological properties as a result of the isolation process[29,30].

In accordance with this latter idea, the so-called phantom burster model introduced by Bertram et al.[31] is able to reproduce slow, fast and medium bursting by changing a single parameter. This flexibility is achieved by incorporating two slow variables working on different time scales. When the fastest of the two slow processes dominate, fast bursting with a period of a few seconds is produced, whereas slow bursting with period of several minutes appears when the slowest variable drive the system. Medium bursting is generated by the interaction of the two slow processes without the need of a third slow variable working on the intermediate time scale, evoking a "phantom" bursting mechanism.

In this work we describe a new mechanism giving rise to phantom bursting, which depends solely on electrical coupling between cells, and does not require changes in single-cell parameters. Consequently, gap-junction coupling alone can prolong the burst period more than tenfold, which provides a novel explanation for the large difference in oscillation frequency between isolated and coupled β-cells.

II. MATHEMATICAL MODELING

We based our study on the mathematical model developed by Bertram et al.[31], which is able to reproduce fast, slow, and intermediate bursting in agreement with experimental

observations in mouse β-cells. The model is described by the differential equations

$$C_m \frac{dV_i}{dt} = -I^i_{ion} - g_c \sum_j (V_i - V_j) \ , \tag{1a}$$

$$\frac{dn_i}{dt} = \frac{n_\infty(V_i) - n_i,}{\tau_n(V_i)} \ , \tag{1b}$$

$$\frac{ds_i}{dt} = \frac{s_\infty(V_i) - s_i}{\tau_s} \ , \tag{2a}$$

$$\frac{dz_i}{dt} = \frac{z_\infty(V_i) - z_i}{\tau_z} \ , \tag{2b}$$

where V_i represents the transmembrane voltage of the i-th cell, n is a gating variable that models the activation of a fast voltage-dependent potassium current, while s and z are gating variables modeling the activation of two slow voltage-sensitive potassium currents that drive the bursting oscillation. Thus, the model is composed of a fast subsystem constituted of the V and n variables described by (1a) and (1b), and a slow subsystem ((2a)–(2b)) describing the slower dynamics of s and z, which – importantly – have time scales that differ by two orders of magnitude. The last term in (1a) models gap-junction coupling to neighboring cells (indexed by j)[20,23,32]. In addition, the model takes into account a voltage-dependent calcium current showing instantaneous activation and no inactivation, and a passive leakage current. The membrane currents are given by

$$\begin{aligned}
I^i_{ion} &= I^i_{Ca} + I^i_K + I^i_s + I^i_z + I^i_L \ , \\
I^i_{Ca} &= g_{Ca} m_\infty (V_i) (V_i - V_{Ca}) , \\
I^i_K &= g_K n_i (V_i - V_K) , \\
I^i_s &= g_s s_i (V_i - V_K) , \\
I^i_z &= g_z z_i (V_i - V_K) , \\
I^i_L &= g_L (V_i - V_L) .
\end{aligned}$$

Table I. Model parameters.

Parameter	Value	Unit
C_m	4524	fF
V_{Ca}	100	mV
V_K	-80	mV
V_L	-40	mV
g_{Ca}	280	pS
g_K	1300	pS
g_s	10	pS
g_z	32	pS
g_L	25	pS
V_n	-9	mV
V_m	-22	mV
V_s	-40	mV
V_z	-42	mV
s_n	10	mV
s_m	7.5	mV
s_s	0.5	mV
s_z	0.4	mV
$\bar{\tau}_n$	9.09	ms
τ_s	1	s
τ_z	120	s

Activation curves and the voltage-dependence of the potassium channel's time constant are described by

$$
\begin{aligned}
n_\infty(V_i) &= \frac{1}{1+\exp\left[(V_n - V_i)/s_n\right]}, \\
m_\infty(V_i) &= \frac{1}{1+\exp\left[(V_m - V_i)/s_m\right]}, \\
s_\infty(V_i) &= \frac{1}{1+\exp\left[(V_s - V_i)/s_s\right]}, \\
z_\infty(V_i) &= \frac{1}{1+\exp\left[(V_z - V_i)/s_z\right]}, \\
\tau_n(V_i) &= \frac{\bar{\tau}_n}{1+\exp\left[(V_i - V_n)/s_n)\right]}.
\end{aligned}
$$

Parameters are given in Tab. I. The model was resolved with the CVODE algorithm in the XPPAUT tool[33], using restrictive settings of numerical tolerances to ensure a good accuracy of results. Bifurcation diagrams were computed with the AUTO package within XPPAUT.

III. RESULTS

We simulated two mutually coupled phantom bursters showing intrinsic fast bursting with a period of ∼5 s, and analyzed emergent electrical activity by varying the coupling conductance g_c in the range 0-60 pS (Fig. 1). As in the uncoupled case ($g_c = 0$ pS), with $g_c \geq 40$ pS, fast bursting behavior with a period of about 5 s can be observed. At $g_c = 60$ pS (Fig. 1(a)), the two cells synchronize completely, and the behavior is as for the single cell. The fast bursting oscillation is driven by oscillations in s while z is almost constant because of its slow dynamics (Fig. 1(b)). At $g_c = 40$ pS the membrane potential oscillations in the active phase of the burst show irregular behavior (Fig. 1(c)), in contrast to the uncoupled case (not shown) and to the coupled system with $g_c = 60$ pS (Fig. 1(a)). Moreover, the underlying s oscillations show slight inter-burst variation in the amplitude (Fig. 1(d)), suggesting that the membrane potential oscillations exhibit variability in the duration of the active phase.

At $g_c = 20$ pS the burst period increases by an order of magnitude to ∼50 s (Fig. 1(e)). As in the original phantom bursting model[31] the s variable reaches a stationary value of ∼1 during the active phase of the burst and decreases to ∼0 in the silent phase, whereas z oscillates in the range $0.6-0.7$ during the burst cycle (Fig. 1(f)). This result suggests that the increase in s does not generate sufficient hyperpolarizing current to achieve cell repolarization and burst termination; therefore z is free to increase, which activates a second repolarizing current that eventually ends the active phase. This scenario is characteristic for phantom bursting[31], but as we will show below, the coupling-induced phantom bursting is mathematically different from the original phantom bursting mechanism in single cells[31].

In order to highlight the range of coupling conductance values that induce phantom bursting and to quantify the increase in burst duration, we computed the burst period varying the coupling strength from 0 to 60 pS (Fig. 1(g)). The burst period increases from about 5 s to a maximum value of ∼55 s at $g_c \simeq 23$ pS. Further increases in g_c cause a non-monotone decrease of the period, which finally converges to the value observed in a fast bursting mode for a coupling conductance higher than 40 pS. This finding suggests that significant changes in the dynamical system occur in response to variations in g_c, and highlights irregular behavior of the electrical oscillations for g_c in the range $25 - 40$ pS, as suggested from the temporal traces of the membrane potential (Fig. 1(c)).

We performed slow-fast analyses[7,31] of the 2-cell system with the aim to dissect the under-

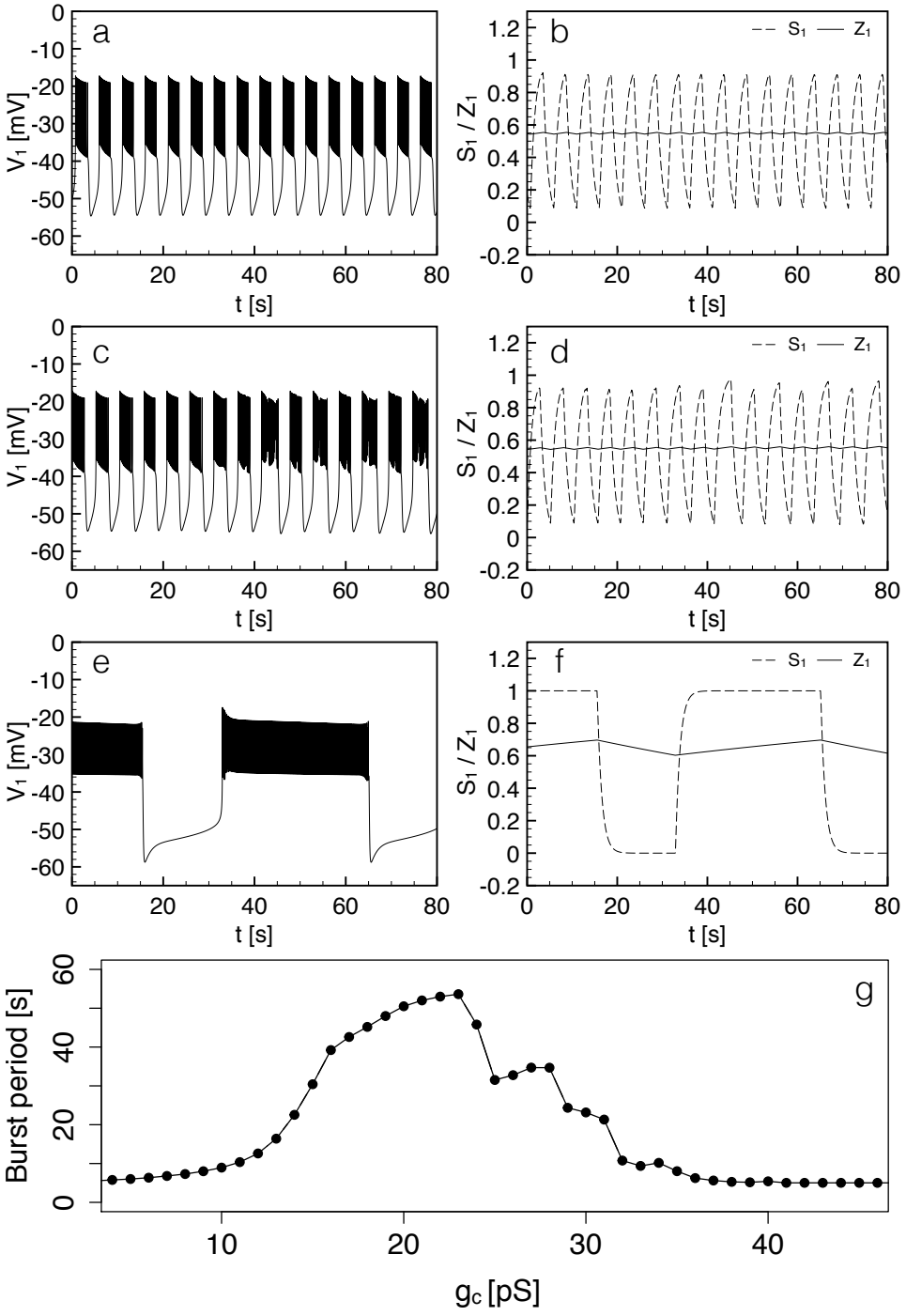

Figure 1. Computed membrane potential (a,c,e) and slow gating variables (b,d,f) of a representative β-cell of a coupled pair of cells. (a,b) $g_c = 60\,\mathrm{pS}$. (c,d) $g_c = 40\,\mathrm{pS}$. (e,f) $g_c = 20\,\mathrm{pS}$. (g) Computed burst period at different values of the coupling conductance g_c.

lying mechanism leading to the coupling-induced changes. In particular, we constructed bifurcation diagrams for the fast subsystem (1) with the slow variables considered as parameters. This procedure is legitimated by the different scales of the dynamics between the fast and the slow processes, which are on the order of milliseconds for the membrane potential and the fast potassium channels gating and on the order of seconds and tens of seconds for the slow variables. Moreover, since the slow variables are in near-perfect synchrony, we make the assumptions $s_1 = s_2 = s$ and $z_1 = z_2 = z$, in line with other published studies[25–27], and further justified in the Appendix. On this basis, we clamped the z variable to a fixed value and treated s as the bifurcation parameter[31], for $g_c = 60$, 40, 20 pS (Fig. 2). In case of fast bursting, we fixed z to its average value, while we used the maximum value of the z-oscillation computed on the full system, to analyze the intermediate bursting mode.

When $g_c = 60$ pS, the fixed points of the fast subsystem fall on a Z-shaped curve composed of a high-voltage branch and a low-voltage branch connected by saddle points (Fig. 2(a)). The low-voltage branch is formed by stable fixed points while the high-voltage branch is characterized by stable fixed points only at very low values of s. These solutions lose stability in a Hopf bifurcation as s increases, which gives rise to stable periodic orbits surrounding the unstable fixed points. At higher values of s, the branch of periodic orbits eventually coalesces with the saddle branch in a homoclinic bifurcation. This diagram is identical to the one computed for an isolated cell[31] and shares common properties with bifurcation diagrams of other models of β-cell activity[7,19,21,25].

By superimposing the s nullcline and reintroducing the dynamics of s, it is possible to explain how fast bursting arises[7,31]. Near the stable low-voltage branch (below the s nullcline) $ds/dt < 0$, so the system moves to the left along the low-voltage branch. When the low-voltage branch disappears through a saddle-node bifurcation, the system jumps to the high-voltage stable periodic solution, above the s nullcline, which is the only stable solution at low values of s. Since $ds/dt > 0$ in this case, the system moves to the right along the high-voltage periodic branch. Eventually, at the homoclinic bifurcation, the system jumps back to the low-voltage stable branch, and another burst cycle can begin. This analysis is confirmed by superimposing the computed trajectories for the two cells coupled with $g_c = 60\,\text{pS}$ (Fig. 2(b)) on the bifurcation diagram. During the active phase, the two cells show identical and synchronized action potential oscillations, and the dynamics is as for an isolated cell. In the following we refer to the high-voltage branch of periodics, underlying

synchronized action potentials firing, as the in-phase (IP) oscillatory branch[25].

At lower values of the coupling conductance the bifurcation diagram shows a more complex behavior. When $g_c = 40\,\text{pS}$ several bifurcations of cycles appear (Fig. 2(c)). When s increases, the in-phase oscillatory branch loses stability through a pitchfork bifurcation generating two stable branches of asymmetric (AS) oscillatory solutions, characterized by low-amplitude and high-amplitude oscillations respectively. These branches lose stability in a torus bifurcation as the bifurcation parameter s increases. Eventually, the asymmetric branches disappear by merging with unstable periodic orbits arising from a second pitchfork bifurcation on the in-phase branch. Before disappearing, the asymmetric branches become stable again via another torus bifurcation. In addition, two other Hopf bifurcations can be noticed on the high-voltage branch of unstable fixed points, through which another branch of oscillatory solutions appears and disappears. This periodic branch represents anti-phase (AP) periodic oscillations in the cells' membrane potentials, with action potentials that are 180 degrees out-of-phase and with identical amplitude. Although this new periodic solution does not affect the emergent dynamics at $g_c = 40\,\text{pS}$, it will play a crucial role at $g_c = 20$ pS as discussed below.

In Fig. 2(d), the superimposed bursting trajectories for the two cells show the effects of the described changes in the fast subsystem bifurcation diagram. Action potential firing within the burst is no longer synchronized. When the system jumps into the high-voltage oscillatory state, it initially follows the unstable in-phase branch but is progressively attracted into a quasi-periodic oscillation at increasing values of the slow variable s. We note that at higher values of s ($\simeq 0.92$), the in-phase branch becomes stable again via a second pitchfork, attracting the nearby trajectories in the phase-space and thus affecting burst termination. As observed for the strongly coupled system, the in-phase branch disappears in a homoclinic bifurcation forcing the trajectories to jump back to the stable low-voltage branch.

When g_c is lowered to 20 pS, a pitchfork branching of the intermediate saddle-branch of the Z-curve and other significant changes are observed (Fig. 2(e)). The right ends of the asymmetric branches no longer coalesce with the in-phase branch, and the anti-phase periodic branch is now shifted to the left. Importantly, this AP branch gains and loses stability via two torus bifurcations. Notably, the AP branch is not present in the single-cell model[31], and hence the mechanism described in the following is a novel path to phantom bursting that appears only in systems of coupled cells.

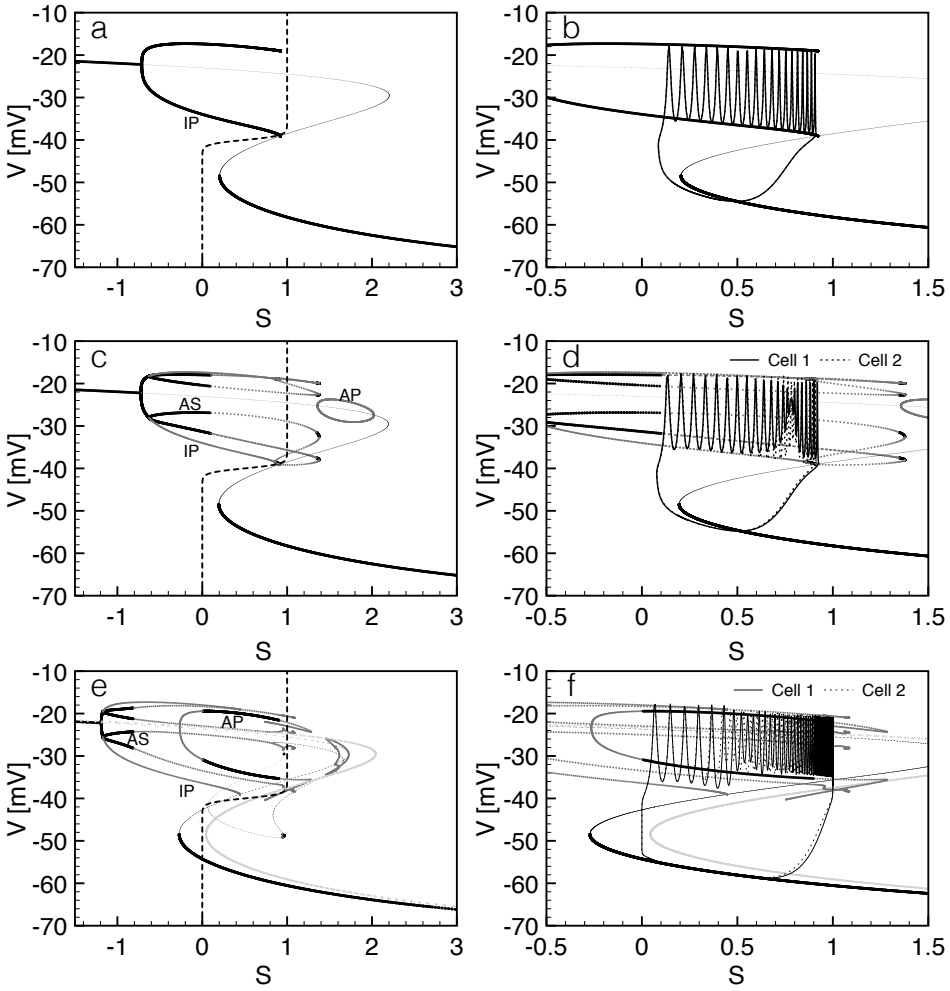

Figure 2. One dimensional fast-subsystem bifurcation diagrams for a 2-cell system with s as bifurcation parameter and fixed z. (a,b) $g_c = 60\,\mathrm{pS}$. (c,d) $g_c = 40\,\mathrm{pS}$. (e,f) $g_c = 20\,\mathrm{pS}$. In (a,b,c,d) z was clamped at 0.55, its mean value in Fig. 1(b,d). In (e,f), bifurcation diagrams were computed for $z = 0.7$, the maximum of the oscillations in Fig. 1(f), while the gray curve indicates the shift of the Z-curve of the bifurcation diagram computed at $z = 0.6$, the minimum of the oscillations in Fig. 1(f). In (a,c,e), the dashed curve is the s-nullcline, $s = s_\infty(V)$, the black thick curves denote stable fixed points and stable periodic orbits, while thin black and dark grey lines indicate unstable fixed points and unstable periodic orbits, respectively. (b,d,f) show numerical solutions overlaid on the bifurcation diagrams.

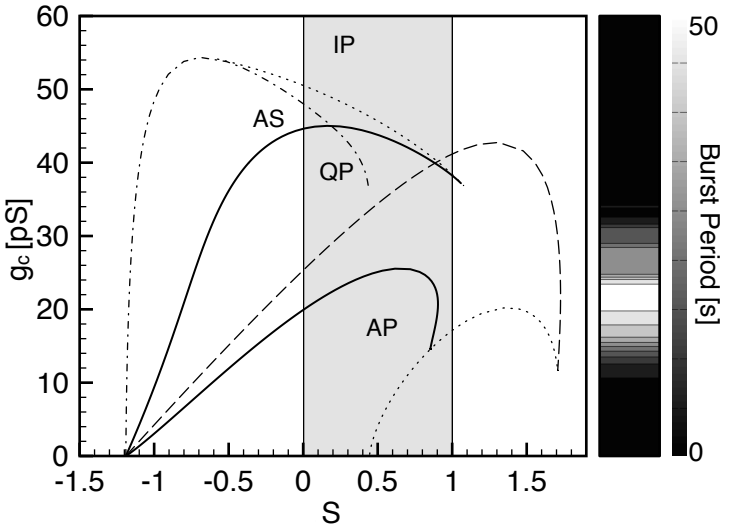

Figure 3. Two-parameter bifurcation diagram computed by varying s and g_c, and reporting the main bifurcations underlying parameter regions with anti-symmetric (AS), anti-phase (AP), quasi-periodic(QP), and in-phase (IP) oscillations. The curves indicate, respectively, pitchfork-of-periodics (dash-dotted), Hopf (dashed), torus (solid), and saddle-node-of-periodics (dotted) bifurcations. The variable z was clamped at 0.7. The light gray area indicates the possible range of variation of s. The color-coded bar to the right of the bifurcation diagram reproduces the burst period of a cell pair for varying coupling strength (from Fig. 1(g)) for easier comparison with the location of the different bifurcations.

The stability of the anti-phase solution is responsible for the increase in the burst period, since it evokes a phantom bursting oscillation. Specifically, at low values of z (approximately < 0.65) the s nullcline intersects the AP branch at $s \approx 1$, when the orbit is stable, thus trapping the system in a sustained oscillation. In other words, the fastest slow s variable is insufficient to terminate the active phase of bursting. In this case, the slower z variable increases since the membrane voltage is sufficiently high to activate the slower potassium current. Increasing or decreasing z cause left or right shifts, respectively, of the whole bifurcation diagram[31], and the increased burst period is due to these slow translations as z increases and decreases. When the system is trapped in the anti-phase oscillatory state, the bifurcation diagram shifts to the left, eventually moving the intersection between the s nullcline and the anti-phase periodic branch into the unstable regime of the AP branch. At this point, the system settles into an irregular motion before escaping to the low-voltage stable branch. Now the s nullcline intersects the low-voltage branch at $s \simeq 0$, thus the trajectory converges to this intersection point, clamping the system in a low-voltage state. However, z is now free to decrease, shifting the bifurcation diagram in the right direction. Eventu-

ally the intersection passes through the saddle-node bifurcation, and the system jumps back into the active phase of bursting. Just after the jump, the trajectory follows the unstable in-phase branch and then settles into the anti-phase oscillation mode after a short transient. Fig. 2(f) shows a complete phantom bursting trajectory for the two cells superimposed on the bifurcation diagram.

To obtain an overview of the geometric structure responsible for the burst period's bell-shaped dependence on coupling strength (Fig. 1(g)), we followed the bifurcations of the periodics in a 2-dimensional bifurcation diagram (Fig. 3). The pitchfork-of-periodics bifurcation giving rise to the AS branches seen in Fig. 2(c) is present for $g_c \lesssim 55$ pS, where its location is nearly insensitive to the value of g_c. For higher g_c values, the cells are completely synchronized and behave as a single cell. The emerging AS branches lose stability in torus bifurcations that lead to quasi-periodic (QP) behavior for $g_c \lesssim 44$ pS. These torus bifurcations are seen in Fig. 2(c), and the QP in the traces for $g_c = 40$ pS in Fig. 1(c,d), but do not modify the burst period much.

The second Hopf bifurcation (HB) leading to anti-phasic (AP) behavior occurs for $g_c \lesssim 42$ pS. The value of the s parameter at which it is located, increases almost linearly with g_c. The emerging periodics gain stability in a torus bifurcation located slightly to the right of the HB, and as discussed above, it is the stability of the AP oscillation in the fast subsystem that permits the slowest z variable to contribute to prolonging the burst period. The torus bifurcation is present for values of g_c below $\sim$24 pS, which coincides nicely with the g_c-value where the burst period is maximal (Fig. 1(g)). The marked drop in the period for $g_c = 25 - 30$ pS is thus likely due to the lack of stability of the AP branch.

IV. CONCLUSIONS

We have shown that diffusive gap junction coupling alone – without introducing cell-to-cell heterogeneity, changes in single-cell parameters, or noise – can explain why electrically coupled β-cells exhibit bursting with a period an order of magnitude greater than isolated cells. Our results show that biological systems may exploit coupling to increase the period of bursting oscillations drastically when these are driven by two slow processes, the one of which being dormant for the single-unit system, via a phantom bursting mechanism. It will be interesting to see whether similar mechanisms underlie the epilepsy-related prolonged

electrical bursts depending on gap junctional coupling[34], or if they are present in other bursting biological, chemical or physical systems.

For the cell pair studied here, we were able to explain the geometrical structure underlying the large increase in burst period. Crucially, and at difference with the single-cell phantom burster scenario[31], gap junction coupling led to the appearance and stability of a branch of anti-phase (AP) solutions[25], which allowed the appearance of phantom bursting and the many-fold increase in burst period. This mechanism is not restricted to the particular single-cell model used here[31], but should appear in any phantom burster model[21,35,36] operating in its fast-bursting mode, as long as gap junction coupling results in a branch of stable periodics, such as the AP solutions found here.

APPENDIX

In this appendix, we justify the assumption $s_1 = s_2$ and $z_1 = z_2$ used in the bifurcation analyses above, and show that the discussion in the main text carries over to the more realistic scenario where the slow variables (s_1 and s_2) differ slightly. The difference $s^\perp = s_1 - s_2$ satisfies

$$\frac{ds^\perp}{dt} = \frac{[s_\infty(V_1) - s_\infty(V_2)] - s^\perp}{\tau_s}, \tag{3}$$

and similarly for $z^\perp = z_1 - z_2$. Our arguments are based on the fact that the two coupled cells are either both in the active or both in the silent phase, except for brief transients, because of relatively strong coupling (Fig. 2) and homogeneity in single cell parameters. As seen from the s-nullcline in Fig. 2, $s_\infty(V) \approx 1$ for any $V > -40$ mV, i.e., during the entire active phase, and $s_\infty(V) \approx 0$ for any $V < -50$ mV, i.e., during the entire silent phase. Consequently, the square bracket in (3) is always close to zero, and it follows that $|s^\perp| \ll 1$ asymptotically. This argument (and a similar one for $z^\perp$) justifies $s_1 \approx s_2$ and $z_1 \approx z_2$, as seen in simulations[25] (Fig. 4). In addition, the bifurcation structure of the fast subsystem is robust to small perturbations away from the diagonal $s_1 = s_2$, i.e. for $0 < |s^\perp| \ll 1$, as shown in Fig. 4. In particular, the stable AP branch is present, and is responsible for the prolonged period seen at $g_c \approx 20$ pS.

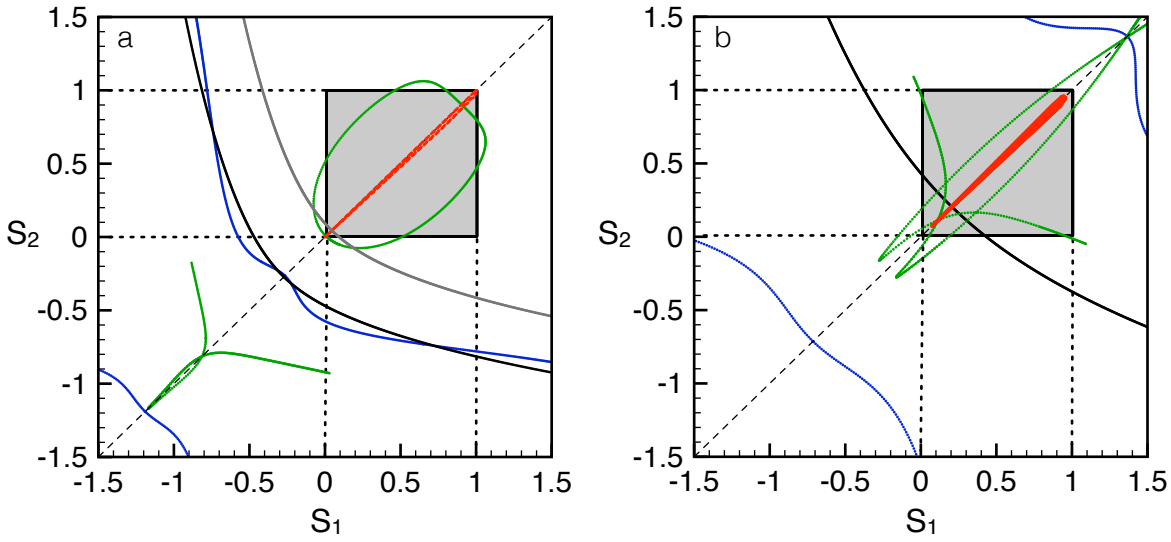

Figure 4. Two-parameter bifurcation diagrams for the fast subsystem with s_1 and s_2 as parameters. Blue, green and black/gray curves indicate Hopf, torus and low-voltage saddle-node bifurcations, respectively. Red curves are simulated trajectories of the full model projected onto the (s_1, s_2) subspace. The light gray area indicates the possible range of variation of s_1 and s_2. The dashed diagonal corresponds to complete synchrony of the slow variables, $s_1 = s_2$. (a) $g_c = 20$ pS and $z_1 = z_2 = 0.7$, i.e. the maximum of the oscillations in Fig. 1(f). In this case, the gray curve indicates the low-voltage saddle-node curve computed at $z_1 = z_2 = 0.6$, i.e. the minimum of the oscillations in Fig. 1(f) occurring at the end of the silent phase (compare with Fig. 2(e)). Note that the torus bifurcations that render the AP stable are robust to perturbations away from the diagonal. (b) $g_c = 40$ pS and $z_1 = z_2 = 0.55$, i.e. its mean value in Fig. 1(b,d). Again, the bifurcation structure is robust to small perturbations away from the diagonal (compare with Fig. 2(c)).

ACKNOWLEDGEMENTS

Research supported by Gruppo Nazionale per la Fisica Matematica (GNFM-INdAM) to A.L., and by the University of Padua (Strategic Research Project "DYCENDI", and Research Project SID (BIRD179302)) to M.G.P.

REFERENCES

[1]K. Bar-Eli and S. Reuveni, J Phys Chem **89**, 1329 (1985).

[2]K. Bar-Eli, Physica D **14**, 242 (1985).

[3]G. Ermentrout and N. Kopell, SIAM J Appl Math **50**, 125 (1990).

[4]K. Tsaneva-Atanasova, C. L. Zimliki, R. Bertram, and A. Sherman, Biophys J **90**, 3434 (2006).

[5]T. Gregor, K. Fujimoto, N. Masaki, and S. Sawai, Science **328**, 1021 (2010).

[6]A. Weber, Y. Prokazov, W. Zuschratter, and M. J. B. Hauser, PLoS One **7**, e43276 (2012).

[7]J. Rinzel, in *Ordinary and Partial Differential Equations*, edited by B. Sleeman and R. Jarvis (Springer-Verlag, New York, 1985) pp. 304–316.

[8]T. R. Chay and J. Keizer, Biophys J **42**, 181 (1983).

[9]J. L. Hindmarsh and R. M. Rose, Proc R Soc Lond B Biol Sci **221**, 87 (1984).

[10]R. J. Butera, Jr, J. Rinzel, and J. C. Smith, J Neurophysiol **82**, 382 (1999).

[11]P. Gilon, M. A. Ravier, J.-C. Jonas, and J.-C. Henquin, Diabetes **51 Suppl 1**, S144 (2002).

[12]R. Bertram, A. Sherman, and L. S. Satin, Am J Physiol Endocrinol Metab **293**, E890 (2007).

[13]P. Rorsman and M. Braun, Annu Rev Physiol **75**, 155 (2013).

[14]N. Pørksen, Diabetologia **45**, 3 (2002).

[15]L. S. Satin, P. C. Butler, J. Ha, and A. S. Sherman, Mol Aspects Med **42**, 61 (2015).

[16]T. A. Kinard, G. de Vries, A. Sherman, and L. S. Satin, Biophys J **76**, 1423 (1999).

[17]A. Tengholm and E. Gylfe, Mol Cell Endocrinol **297**, 58 (2009).

[18]I. Atwater, L. Rosario, and E. Rojas, Cell Calcium **4**, 451 (1983).

[19]A. Sherman, J. Rinzel, and J. Keizer, Biophys J **54**, 411 (1988).

[20]A. Sherman and J. Rinzel, Biophys J **59**, 547 (1991).

[21]M. G. Pedersen, J Theor Biol **248**, 391 (2007).

[22]M. G. Pedersen and M. P. Sørensen, SIAM J Appl Math **67**, 530 (2007).

[23]A. Loppini, A. Capolupo, C. Cherubini, A. Gizzi, M. Bertolaso, S. Filippi, and G. Vitiello, Physics Letters A **378**, 3210 (2014).

[24]A. Sherman and J. Rinzel, Proc Natl Acad Sci U S A **89**, 2471 (1992).

[25]A. Sherman, Bull Math Biol **56**, 811 (1994).

[26]G. De Vries and A. Sherman, J Theor Biol **207**, 513 (2000).

[27]M. G. Pedersen, J Theor Biol **235**, 1 (2005).

[28]P. Smolen, J. Rinzel, and A. Sherman, Biophys J **64**, 1668 (1993).

[29]S. Göpel, T. Kanno, S. Barg, J. Galvanovskis, and P. Rorsman, J Physiol **521 Pt 3**, 717 (1999).

[30]P. Rorsman, L. Eliasson, T. Kanno, Q. Zhang, and S. Gopel, Prog Biophys Mol Biol **107**, 224 (2011).

[31]R. Bertram, J. Previte, A. Sherman, T. A. Kinard, and L. S. Satin, Biophys J **79**, 2880 (2000).

[32]A. Loppini, M. Braun, S. Filippi, and M. G. Pedersen, Phys Biol **12**, 066002 (2015).

[33]G. Ermentrout, *Simulating, analyzing, and animating dynamical systems: A guide to XPPAUT for researchers and students* (SIAM Books, Philadelphia, 2002).

[34]R. Köhling, S. J. Gladwell, E. Bracci, M. Vreugdenhil, and J. G. Jefferys, Neuroscience **105**, 579 (2001).

[35]T. R. Chay, Biophys. J. **73**, 1673 (1997).

[36]R. Bertram and A. Sherman, Bull Math Biol **66**, 1313 (2004).